JOURNAL OF Materials CHEMISTRY

Structural, magnetic and lithium insertion properties of spinel-type $Li_2Mn_3MO_8$ oxides (M = Mg, Co, Ni, Cu)

P. Strobel,[a] A. Ibarra Palos,[a] M. Anne[a] and F. Le Cras[b]

[a]*Laboratoire de Cristallographie CNRS, BP 166, 38042 Grenoble Cedex 9, France. E-mail: strobel@labs.polycnrs-gre.fr*
[b]*DEM/LSE, Commissariat à l'Energie Atomique, 38054 Grenoble Cedex 9, France*

Received 23rd July 1999, Accepted 20th October 1999

Single-phase compounds $Li_2Mn_3MO_8$ (M = Mg, Co, Ni, Cu) have been synthesized and investigated as replacements of $LiMn_2O_4$ for lithium intercalation below 3 V. They all retain the spinel structure, with cation ordering on the octahedral M (16d) site for M = Mg only. Cell parameters vary as Co < Ni < Mg ≈ Cu < Mn and average M–O bond lengths as Co ≈ Ni < Cu < Mg < Mn. Lithium was intercalated both chemically and electrochemically. Electrochemical potential step spectroscopy shows features typical of a two-phase intercalation reaction, in spite of a manganese valence range mostly above the accepted Jahn–Teller distortion limit (50% Mn^{3+}). The tetragonal distortion is only noticeable at high intercalation levels. It yields *c*/*a* distortion values much lower for M = Co or Ni than for unsubstituted $LiMn_2O_4$. However, no improvement in electrochemical cyclability was obtained. Magnetic susceptibility measurements show features typical of frustrated systems, as expected for the 16d sublattice, and confirm that chemical intercalation reaches lithium contents close to the theoretical limit (one additional Li per AB_2O_4 formula unit). For cobalt substitution, bond length and Curie constant analysis both lead to a charge distribution $Li_2[(Mn^{4+})_2Mn^{3+}Co^{3+}]O_8$ rather than $Li_2[(Mn^{4+})_3Co^{2+}]O_8$.

1 Introduction

Li–Mn–O spinel compounds are among the most widely studied materials for secondary lithium batteries.[1,2] The normal spinel $LiMn_2O_4$ is a mixed-valence compound which can give rise to the following reactions in lithium batteries:

lithium insertion:

$$\underset{\text{cubic, } Fd3m}{Li[Mn^{4+}Mn^{3+}]O_4} \rightleftarrows \underset{\text{cubic, } Fd3m}{\square[Mn^{4+}Mn^{4+}]O_4} + Li \quad (1)$$

lithium extraction:

$$\underset{\text{cubic, } Fd3m}{Li[Mn^{4+}Mn^{3+}]O_4} + Li \rightleftarrows \underset{\text{tetragonal, } I4_1/amd}{Li_2[Mn^{3+}Mn^{3+}]O_4} \quad (2)$$

where square brackets denote species in octahedral B sites, as is usual in spinel crystal chemistry. These reactions occur at potentials *ca.* 3 or 4 V *vs.* Li/Li^+ in non-aqueous electrolyte, respectively.

As shown in this scheme, the 3 V reaction is accompanied by a structural transition from cubic to tetragonal, which occurs when the fraction of Mn^{3+} is > 50%.[1,3] This effect is due to the Jahn–Teller effect, which is an inherent property of the Mn^{3+} ion in octahedral coordination (electron configuration $t_{2g}^3e_g^1$). This distortion is believed to be a major factor in the large capacity drop of $LiMn_2O_4$-based lithium batteries cycled at 3 V,[1] and to a lesser extent at 4 V, because $LiMn_2O_4$ is on the verge of the structural transition. In fact, a recent electron microscopy study showed the presence of grains of tetragonal phase in $LiMn_2O_4$ at the end of discharge after cycling above 3.3 V,[4] and stoichiometric $LiMn_2O_4$ itself undergoes a slight tetragonal distortion when cooled below room temperature.[5]

A close look at the charge distributions in reactions (1) and (2) shows that only half the manganese atoms are active in each of these redox processes. Consequently, the range of manganese valences covered in these reactions can be modified by appropriate substitutions on the 'inactive' manganese fraction. The most obvious case is the solid solution $Li_{1+\alpha}Mn_{2-\alpha}O_4$, where an increase in α raises the initial manganese valence v(Mn) and allows reaction (2) to proceed partly above the v(Mn) = 3.5 limit. Several groups showed that performances on the 3 V plateau can indeed be enhanced using a starting $Li_{1+\alpha}Mn_{2-\alpha}O_4$ host with $\alpha > 0$, *i.e.* higher initial v(Mn).[6,7]

In the more general case of a substitution by yM^{n+} for Mn (formula $Li_{1+x}[M^{n+}{}_yMn_{2-y}]O_4$), the manganese valence varies as $v(Mn) = (7-x-ny)/(2-y)$ with an intercalation range $0 \leqslant x \leqslant 1$.

This variation is plotted for $n = 2$ in Fig. 1, showing that the substitution has a double effect : (i) an increase in initial manganese valence with y, (ii) a slight increase in the slope of

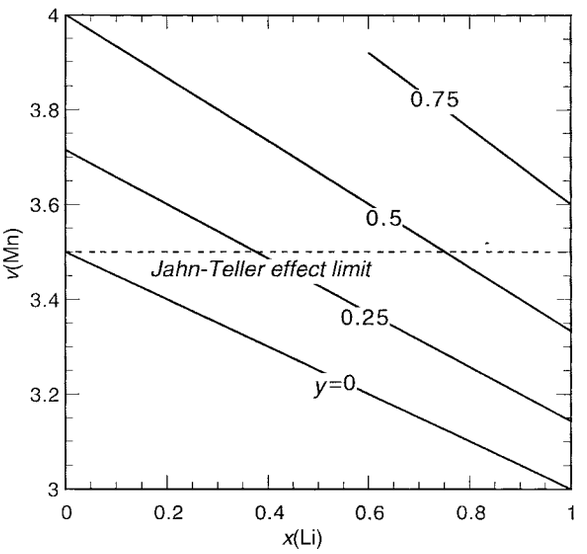

Fig. 1 Evolution of the manganese valence v(Mn) on lithiation for different substitution levels of divalent cation in the formula $Li_{1+x}[Mn_{2-y}M^{2+}{}_y]O_4$.

This journal is © The Royal Society of Chemistry 2000

$v(\mathrm{Mn}) = f(x)$, due to the decrease in Mn fraction $(2-y)$ in the spinel formula unit with increasing y.

The substitution ratio $y = 0.5$ seems particularly interesting: it gives an initial material containing Mn^{4+} only, and allows the intercalation of 0.75 Li while staying above the $v(\mathrm{Mn}) = 3.5$ tetragonal distortion limit.

We previously studied the compound $Li[Mn_{1.5}Mg_{0.5}]O_4$ (or $Li_2Mn_3MO_8$).[8] It exhibits a complex intercalation behaviour with a succession of two- and one-phase intercalation reactions. Improvements in electrochemical performances for smaller fractions of Co or Ni were reported by a number of groups, notably Sánchez *et al.* regarding the 3 V lithium insertion reaction.[9,10] We are aware of only one report of electrochemical studies using the $Li_2Mn_3MO_8$ stoichiometry, by Amine *et al.* for M = Ni.[11] We examine here the structural and lithium intercalation properties of $Li_2Mn_3MO_8$ with M = Mg, Co, Ni or Cu.

2 Experimental

The title compounds were synthesized by solid state reaction. Appropriate mixtures of reagent-grade carbonates or acetates were repeatedly fired in alumina crucibles for $\geqslant 15$ h periods at 700 °C under oxygen atmosphere, with intermittent grinding. The moderate temperature and oxygen atmosphere were used in order to ensure a maximum manganese valence v(Mn) in the spinel phases formed, based on the experience acquired on the $Li_{1+\alpha}Mn_{2-\alpha}O_4$ system. In that study, we found that single-phase compounds with high v(Mn), *i.e.* high α values, decompose at higher temperatures into spinel phases with lower v(Mn) and Li_2MnO_3 impurity.[7,12] An optimum reaction temperature of 750 °C for the synthesis of $Li_2Mn_3CuO_8$ was reported elsewhere.[13]

Samples were analyzed by X-ray diffraction using a Siemens D-5000 powder diffractometer equipped with a diffracted-beam graphite monochromator, rotating sample holder and operated with Cu-Kα radiation. The structures were refined from low-counting time diffraction data ($\geqslant 50$ s step^{-1}) using the Rietveld method (FULLPROF program[14]).

Electrochemical tests were carried out in liquid electrolyte at room temperature using 24–30 button cells. The electrolyte was a 1 M solution of $LiClO_4$ in propylene carbonate (PC)–ethylene carbonate (EC)–dimethoxyethane (DME) (1 : 1 : 2). Positive electrodes were cut from mixtures of the dried oxide powder with 20% carbon black (Y50 grade, SNNA, Berre, France) and 10% PTFE. Typical quantities of active material used in electrochemical cells were 25–50 mg. The negative electrode was 200 μm-thick lithium foil (Metall Ges., Germany). No reference electrode was used because the potential is essentially constant at the anode interface. Cells were assembled in a glove box under argon with <1 ppm H_2O. Electrochemical studies were carried out using a MacPile controller (BioLogic, Claix, France), either in galvanostatic mode (for repeated cyclings) or in step-potential electrochemical spectroscopy (SPES),[15,16] using typically 10 mV h^{-1} potential steps.

In order to ensure the availability of gram-scale amounts of fully lithiated samples for further structural and magnetic studies, chemical lithiation experiments were carried out on the Co, Ni and Cu compounds using a proprietary procedure of CEA, Grenoble,[17] which is milder and easier to carry out than the classical butyllithium route.

Static magnetic susceptibility and magnetization measurements were carried out using an extraction magnetometer (L. Néel Lab., Grenoble) in the temperature range 4–300 K, usually in a field of 0.1 T. Selected samples were also measured in the range 300–800 K.

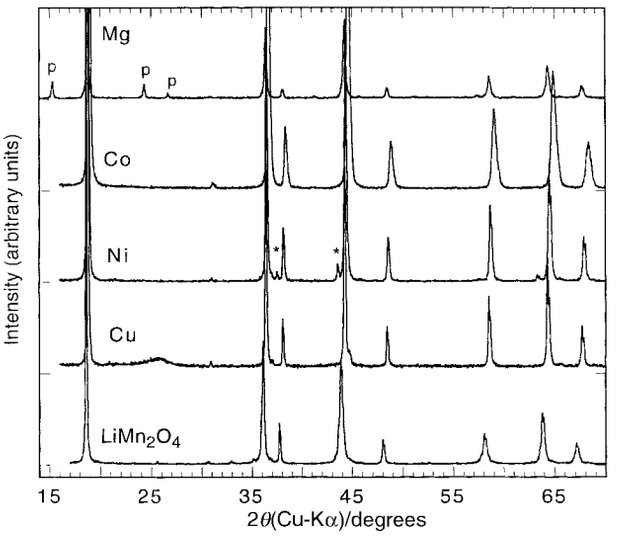

Fig. 2 X-Ray powder patterns of $Li_2Mn_3MO_8$ (M = Mg, Co, Ni, Cu, Mn) (top to bottom). p: reflections due to a primitive cubic cell (see text); *: NiO reflections.

3 Results

3.1 Synthesis and structural characterization

X-Ray powder patterns of $Li_2Mn_3MO_8$ compounds are shown in Fig. 2. For M = Co, Ni and Cu, all observed reflections are indexible in the spinel structure (*Fd3m* space group), with the exception of traces of NiO in the case of nickel (see asterisks in Fig. 2). This result confirms previous studies,[11,18] which showed that pure $Li_2Mn_3NiO_8$ could not be obtained by solid-state reaction. However, the NiO content found here is low (1.7 wt%, from a two-phase structural refinement) and its influence on electrochemical results is probably negligible.

The diffraction pattern of $Li_2Mn_3MgO_8$ (Fig. 2, top) displays numerous additional reflections, which can be indexed using a primitive cubic cell instead of the face-centered spinel one. This lowering of symmetry is due to an ordering of the cations on the octahedral (16d) sites of the spinel structure[19] and results in a $P4_332$ space group. The results of structure refinements are summarized in Tables 1 and 2. The cell parameters obtained are in good agreement with previously reported values. All substitutions investigated induce a decrease in the cell parameter a, and have little effect on the oxygen parameter. Rietveld refinements confirmed that all substituents investigated occupy 16d sites. The very weak, but visible 220 peaks (at $2\theta \approx 31°$ in Fig. 2), prompted to us to test a partial occupation of tetrahedral (8a) sites by M atoms: the resulting occupation was <0.015 in all cases. Our $Li_2Mn_3CuO_8$ sample, in particular, differs in this respect from that investigated by Ein-Eli *et al.*, which was obtained by a sol–gel technique[13] and found to contain 10% copper on tetrahedral sites.

The evolution of M–O distances with substitution (see Table 1) shows the combined influence of two effects: (i) the size of the substituant atom, (ii) the change in manganese valence v(Mn). The former effect concerns 1/4 of the octahedral site cations, the latter 3/4. The fact that a (and the M–O distance) decreases when replacing a fraction of Mn by larger cations (Mg, Ni, Cu) shows that the manganese valence change effect is prevailing: on substitution by M^{2+}, v(Mn) is increased from $+3.5$ to $+4$, corresponding to an average Mn ionic radius 0.585 and 0.53 Å, respectively. Cobalt substitution decreases the M–O distances most, suggesting the presence of Co^{3+} rather than Co^{2+} in the structure. This has been confirmed by magnetic susceptibility measurements (see section 3.4). Finally, we note that, in spite of a larger size difference, nickel and copper do not induce cation ordering on the 16d sites as magnesium does.

Table 1 Structural data for $Li_2Mn_3MO_8$ compounds, as determined by Rietveld refinement

M	Ionic radius[20] /Å		Space group	Cell parameter/Å		Oxygen parameter[a]	B^{iso}/Å^2		M–O distance /Å	Refinement parameters			
				Literature	This work		Oxygen	Octahedral cations		$N-P+C$	R_{wp}	χ^2	R_{Bragg}
Mn[b]	3+	0.64	*Fd*3*m*		8.2449(2)	0.2632(3)			1.958 × 6	—[c]			
	4+	0.53											
Mg	2+	0.67	$P4_332$ (spinel super structure)	8.183[22]	8.1869(4)	—[d]	3.0(1)	2.29(6)	Mn: 1.881 × 2 1.919 × 2 1.940 × 2 Mg: 2.062 × 6	3977	15.4	1.37	3.34
Co	2+	0.74	*Fd*3*m*	8.13[19]	8.1379(2)	0.2629(2)	1.36(9)	0.65(4)	1.935 × 6	2307	11.7	1.79	2.20
	3+	0.61											
Ni[e]	2+	0.69	*Fd*3*m*	8.174[11] 8.163[18]	8.1667(2)	0.2634(2)	1.70(13)	0.79(6)	1.938 × 6	1854	14.5	1.67	2.35
Cu	2+	0.73	*Fd*3*m*	8.192[13]	8.1888(2)	0.2633(3)	1.38(12)	0.89(6)	1.944 × 6	1647[b]	9.50	2.17	2.91

[a]Only variable atomic coordinate in the spinel structure (cubic, $Z=4$). [b]Parent compound $LiMn_2O_4$, included for reference. [c]See ref. 21. [d] See Table 2. [e]Two-phase refinement; this sample contains 1.7 wt% NiO.

3.2 Electrochemical behaviour

Fig. 3 shows SPES slow-scanning voltammograms of $Li_2Mn_3MO_8$ (M = Mn, Co, Ni, Cu) in the range 2.2–3.5 V. All samples exhibit one main reversible current peak corresponding to lithium insertion/extraction from the spinel structure. The reduction and oxidation peaks for a given sample do not overlap, but have a common starting potential [see enlargement in Fig. 3(b)]. This behaviour is typical of a two-phase reaction.[23] It is observed on all samples, showing that an increase in initial manganese valence from $Mn^{3.5+}$ to Mn^{4+} does not modify the basic features of lithium intercala-

Table 2 Refined atomic positions for $Li_2Mn_3MgO_8$ (space group $P4_332$)

Atom	Position	x	y	z	B_{iso}/Å^2
Li	8c	0.01(3)	0.01(3)	0.01(3)	1.40(5)
Mg	4b	5/8	5/8	5/8	2.29(6)
Mn	12d	1/8	0.3799(3)	0.8701(3)	2.29(6)
O1	8c	0.384(1)	0.384(1)	0.384(1)	3.0(1)
O2	24e	0.1249(5)	0.1500(9)	0.8584(7)	3.0(1)

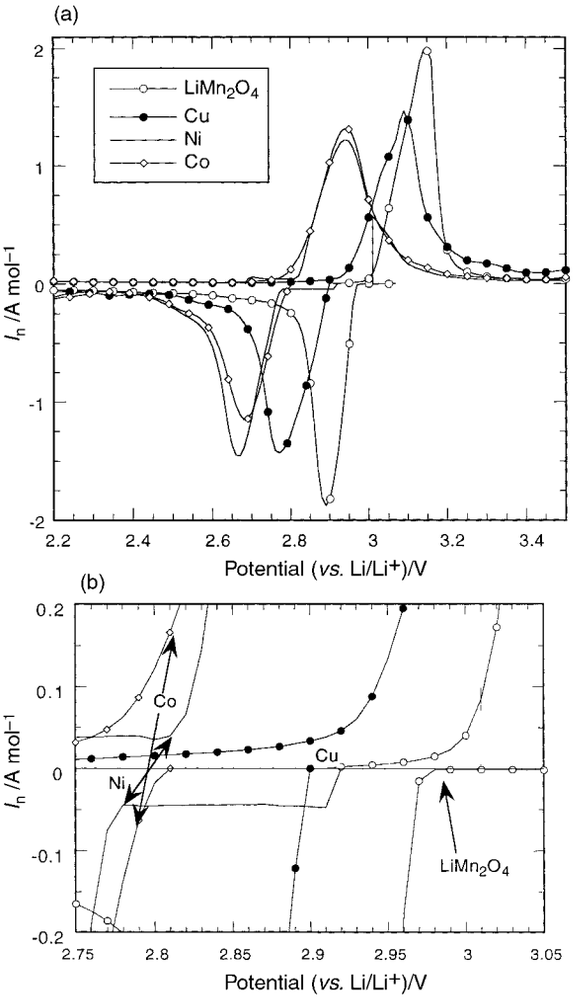

Fig. 3 (a) SPES voltammograms of $Li_2Mn_3MO_8$ (M = Mn, Co, Ni, Cu) recorded in lithium button cells at 10 mV h^{-1}. Currents have been normalized to the amount of sample. (b) Enlargement of the central area of (a), showing the definition of the equilibrium potentials (arrows).

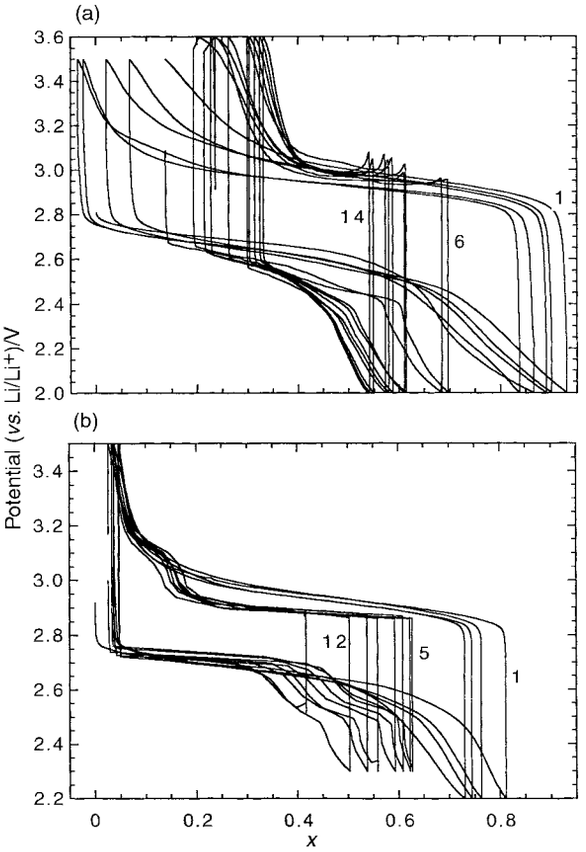

Fig. 4 Charge–discharge cycling of $Li_2Mn_3CoO_8$ (a) and $Li_2Mn_3NiO_8$ (b). The first five (Co), four (Ni) cycles were monitored potentiostatically at 10 mV h^{-1} steps, the following ones galvanostatically at $\approx C/40$ rate. Relevant cycle numbers are indicated. The x scale refers to the spinel formula unit, *i.e.* $Li_{1+x}M_2O_4$.

tion in Li–Mn–O spinel. However, substitution induces a slight shift in potential, in the order $U(\mathrm{Co}) \approx U(\mathrm{Ni}) < U(\mathrm{Cu}) < U(\mathrm{Mn})$. The equilibrium potentials U_{eq} at 25 °C [interpolated between reduction and oxidation waves in Fig. 3(b)] are as follows (± 5 mV): Mn 2.98 V, Cu 2.91 V, Mg 2.81 V (ref. 7), Co, Ni 2.795 V.

These potentials scale well with average M–O distances, which increase in the order Co ≈ Ni < Cu < Mn, if one ignores the Mg case, where Mg and Mn occupy distinct structural sites.

$LiMg_{0.5}Mn_{1.5}O_4$[8] shows a similar main reversible two-phase peak, but this is followed on reduction by two other reactions centered at 2.25 and *ca.* 1.80 V, each accounting for about half of the capacity of the first peak. No such reactions was observed on the other samples: as shown in Fig. 3(a), the current–voltage curves for M = Co, Ni, Cu are very flat in the 2.25 V range.

Examples of galvanostatic cycling are shown in Fig. 4. The length of the 3 V plateau decreases steadily, even at low cycling rates (here $\approx C/40$, *i.e.* full discharge in 40 h). In addition, the voltage plateau shows an increasingly sharp break at 2.4–2.5 V, which is ascribed to kinetic limitations. In fact, even at such low charge/discharge rate, the system is far from equilibrium under the galvanostatic regime. A clear evidence for this is the fast jump in potential observed on relaxation at the end of each discharge: U goes back to 2.70 V within 2–3 h, with an increasing initial slope of $U(t)$ with increasing cycle number (see Fig. 5). In the galvanostatic regime, these materials show no improvement with respect to unsubstituted $LiMn_2O_4$, in spite of the increase in initial manganese valence induced by cationic substitution (see Fig. 6). For M = Ni, this result differs markedly from that obtained recently by Amine *et al.*,[11] who found a much lower capacity drop using a $Li_2Mn_3NiO_8$ sample prepared by a sol–gel technique. This difference shows that the much smaller grain size and/or larger specific surface area of the sol–gel sample is probably a major factor in the cycling performances.

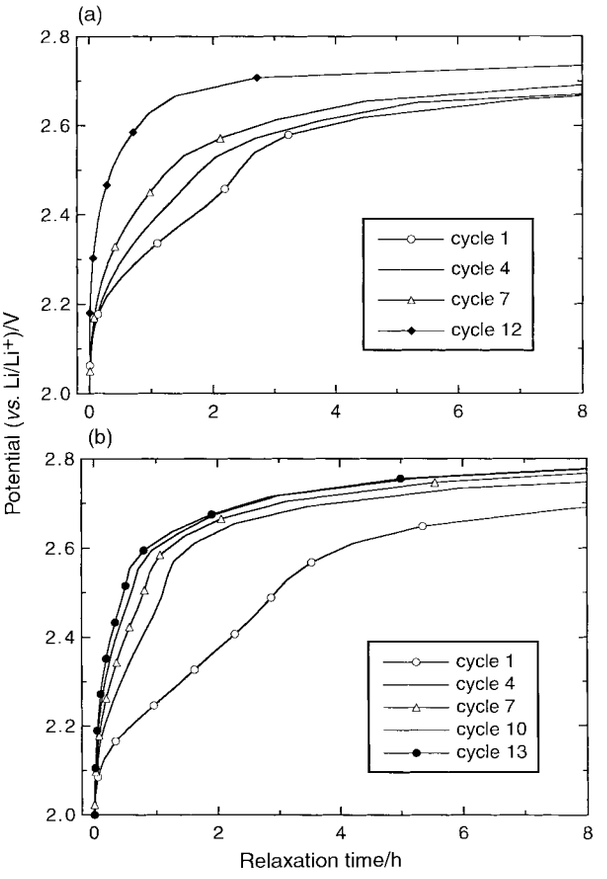

Fig. 5 Evolution of potential on relaxation at the end of discharge at 2.0 V at different charge–discharge cycles for $Li_2Mn_3CoO_8$ (a) and $Li_2Mn_3NiO_8$ (b).

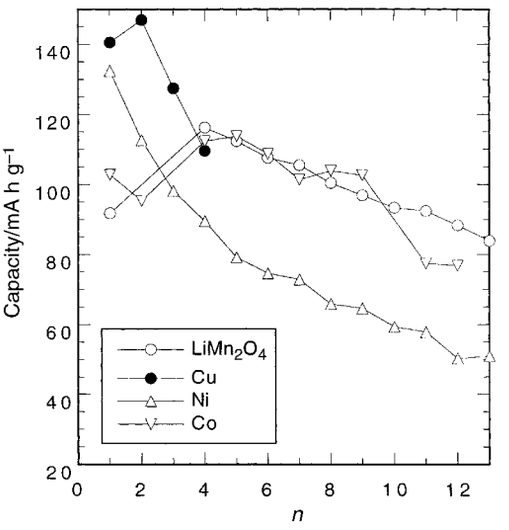

Fig. 6 Evolution of the cathode capacity as a function of the number of charge–discharge cycles n for various $Li_2Mn_3MO_8$ compounds.

The positive electrode pellets of several electrochemical cells were submitted to X-ray diffraction after cycling. As shown in Fig. 7 and 8, the X-ray diffraction patterns obtained after discharge at 2.0–2.4 V show hardly any difference with respect to the host (neglecting contributions from the sample holder). Very weak and broad additional lines, which can be ascribed to a tetragonally-distorted spinel, are observed in a few cases only, for instance a $Li_2Mn_3CuO_8$ cell discharged to $x \approx 0.90$ (Fig. 8, middle).

Such a behaviour, which is *a priori* surprising since SPES showed clearly two-phase behaviour in all cases, can be explained as follows. With an initial stoichiometry $Li_2Mn_3M^{2+}O_8$, the theoretical limit of intercalation corresponds to a manganese valence $v(\mathrm{Mn}) = 3.33$, whereas these materials can be discharged to $x(\mathrm{Li}) = 0.75$ without crossing the Jahn–Teller distortion limit $v(\mathrm{Mn}) = 3.50$ (Fig. 1). Experimentally, x(Li) is found to drop below 0.75, which is equivalent to

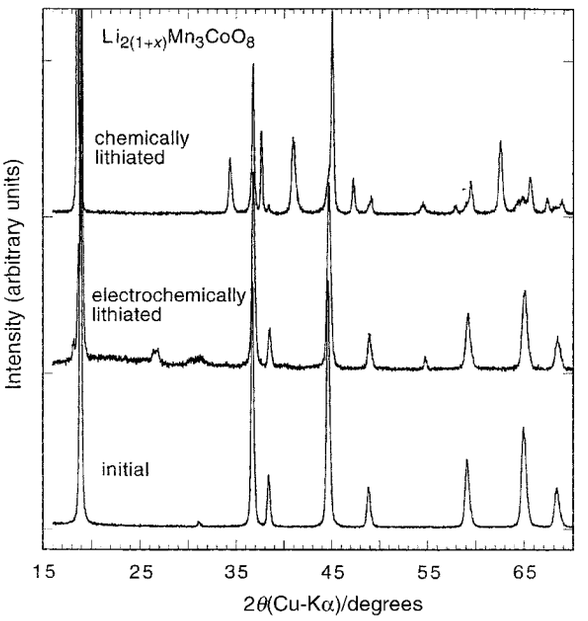

Fig. 7 X-Ray powder patterns (Cu-Kα radiation) of $Li_2Mn_3CoO_8$ and its lithiated derivatives. From bottom to top: initial sample, electrochemically lithiated pellet discharged down to 1.86 V ($x = 0.86$), chemically lithiated powder. Arrows indicate the strongest additional reflections ascribed to a tetragonally-distorted spinel.

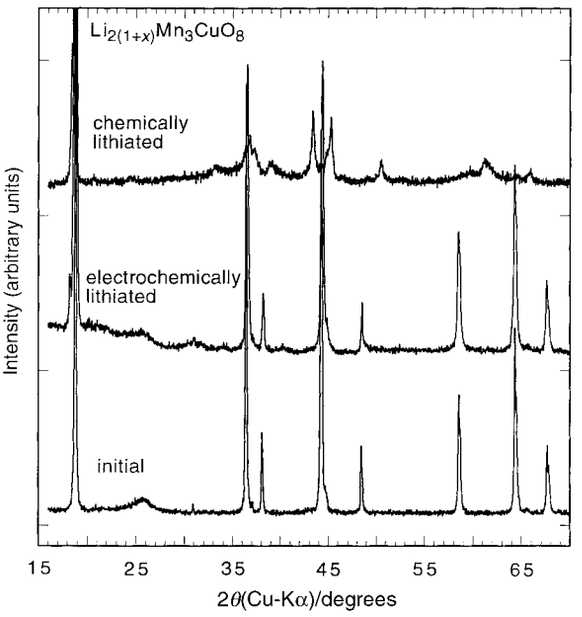

Fig. 8 X-Ray powder patterns (Cu-Kα radiation) of $Li_2Mn_3CuO_8$ and its lithiated derivatives. From bottom to top: initial sample, electrochemically lithiated pellet discharged down to 2.0 V ($x=0.92$), chemically lithiated powder.

108.6–110.0 mA h g^{-1}, for a few cycles only, as shown by Fig. 4 and 6. Consequently, no tetragonal distortion is expected to occur in such cells. A similar result was obtained for the first reduction peak in $Li_2Mn_3MgO_8$ (ref. 8).

It remains to reconcile this apparently constant unit cell with the SPES results. A remarkable example of a similar behaviour is the titanium spinel $Li_{4+x}Ti_5O_{12}$ system, which shows a very flat, two-phase like lithiation potential with negligible change in cell volume.[24] This problem was solved recently by Scharner *et al.*,[25] who analyzed carefully high-angle diffraction data and indeed found a two-phase system with a cell parameter change of 0.0057 Å, *i.e.* 0.07%. A similar mechanism can be proposed here: for $Li_2Mn_3MgO_8$ with M = Mg and Ni, we observed a cell parameter increase of *ca.* 0.006 Å. Fig. 9 shows an example of the slight line shift observed on high-angle diffraction patterns for $Li_2Mn_3NiO_8$.

3.3 Chemical lithium intercalation

The X-ray powder patterns of chemically lithiated samples are compared to those of the initial compounds and the electrochemically discharged ones in Fig. 7 and 8. The chemical route clearly produces tetragonally-distorted spinels (hausmannite-type structure, space group $I4_1/amd$). All lithiated samples still contained a fraction of cubic spinel phase. These were estimated from two-phase structural refinements for $Li_2Mn_3CoO_8$ and $Li_2Mn_3NiO_8$, and found to lie in the range 5–6%. The evolution of structural parameters is summarized in Table 2. The copper-substituted phase is rather atypical: it shows broad reflections, and is the only sample for which the cell volume variation ΔV is markedly different from that observed for $LiMn_2O_4$. Other substitutions give rise to ΔV values comparable to $LiMn_2O_4$, but differ considerably in the magnitude of tetragonal distortion. This point is addressed further in section 4.

3.4 Magnetic behaviour

Magnetic susceptibilities of the $Li_2Mn_3MO_8$ series are shown in Fig. 10–13. All but lithiated $Li_2Mn_3CuO_8$ could be fitted with a Curie–Weiss law in a high enough temperature range; most samples were measured both below and above room temperature. The values of Curie constant C and θ are given in Table 3.

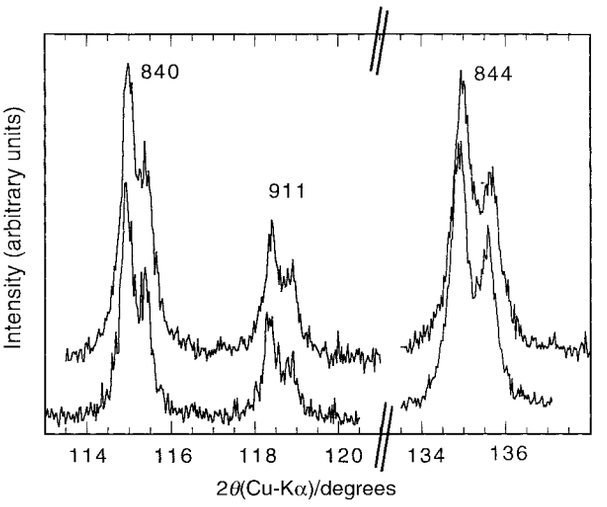

Fig. 9 High-angle reflections of $Li_2Mn_3NiO_8$ (bottom) and its electrochemically lithiated derivative (top).

No shoulder or kink is observed at temperatures corresponding to possible magnetic impurities, such as Li_2MnO_3 ($T_N=36.5$ K), Mn_3O_4 ($T_C=49$ K) or Mn_2O_3 ($T_N=80$ K).[26] However, lithiated samples showed nonlinear $\chi^{-1}(T)$ variation above *ca.* 500 K (see Fig. 11 and 12, insets). This behaviour is ascribed to decomposition of the unstable lithiated spinel structure. We showed recently that chemically lithiated $Li_2Mn_2O_4$ decomposes at *ca.* 650 K into a stoichiometric spinel and the lithium-rich phase Li_2MnO_3.[27]

Magnetic data for unsubstituted $LiMn_2O_4$ are included in Table 3 for comparison. Our results for this compound are in good agreement with literature data, giving θ values in the range -260 to -273 K.[19,28–30]

Turning now to substituted samples, the simplest case is $Li_2Mn_3MgO_8$, with a non-magnetic substituent and tetravalent manganese only. The θ value is slightly positive, indicating the presence of ferromagnetic interactions. Order sets in only at temperature <10 K (see Fig. 10). The Curie constant is in excellent agreement with that expected for a tetravalent Mn compound (see Table 3). Note that this behaviour is quite different from that of the defect spinel λ-MnO_2, which has $\theta=-104$ K.[31] The ordered replacement of one quarter of the

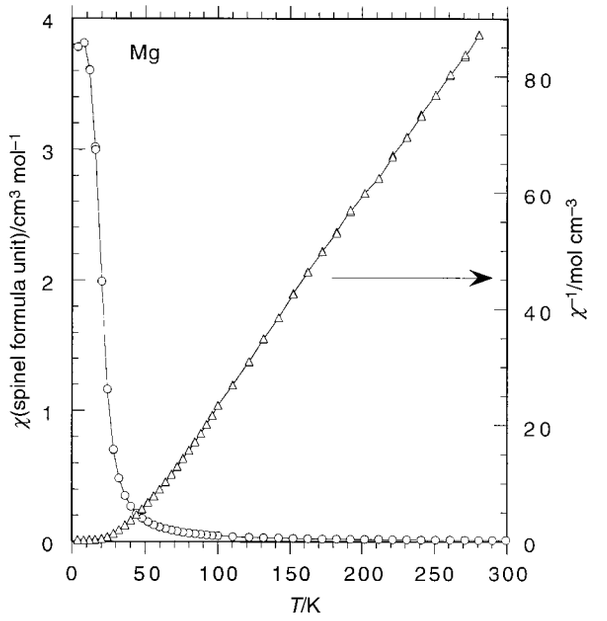

Fig. 10 Temperature dependence of the molar magnetic susceptibility of $Li_2Mn_3MgO_8$ in a 0.1 T field.

Table 3 Crystallographic data for chemically lithiated $Li_{2(1+x)}Mn_3MO_8$ compounds

	Initial		Lithiated					
M	a/Å	V/Å^3	a_{cub}[a]/Å	c/Å	V[a]/Å^3	c/a	$\triangle V$ (%)	Comments
Mn	8.2449(2)	560.47(4)	7.9943(3)	9.2415(5)	590.61(8)	1.156	+5.38	
Mg	8.1869(4)	548.73(8)	8.158(4)	8.693(3)	578.5(8)	1.066	+5.43	Electrochemical lithiation, $x=0.7$[8]
Co	8.1379(2)	538.94(4)	8.0506(4)	8.8086(5)	570.91(8)	1.094	+5.93	+5% cubic spinel
Ni	8.1667(2)	544.68(4)	8.0852(4)	8.7549(7)	572.3(1)	1.083	+5.07	+6.5% cubic spinel
Cu	8.1888(2)	549.11(4)	8.012(3)	9.289(9)	596(1)	1.159	+8.58	Broad reflections, +cubic spinel

[a]Referring to the spinel cubic cell; in the Hausmannite-type I-centered tetragonal cell, $a_{tet}=a_{cub}/\sqrt{2}$.

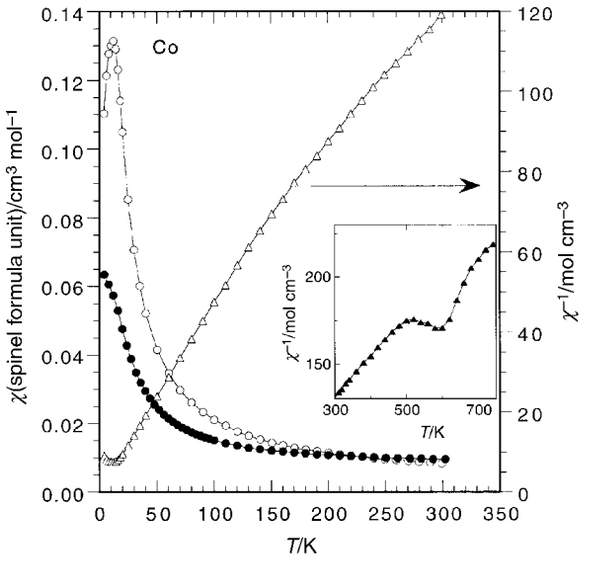

Fig. 11 Temperature dependence of the molar magnetic susceptibility of $Li_{2(1+x)}Mn_3CoO_8$ in a 0.1 T field. Open symbols: $x=0$, closed symbols: $x=1$. Inset: susceptibility data for lithiated sample up to 750 K.

Mn^{4+} ions by non-magnetic Mg^{2+} thus changes considerably the magnetic interactions in the 16d sublattice.

All other compounds studied, where no cationic order was detected, have negative θ values. The cobalt case is peculiar, since several charge distributions can be considered. As shown in Table 4, the best agreement with the Curie constant is found for formula $Li_2[(Mn^{4+})_2Mn^{3+}Co^{3+,LS}]O_8$. Such a distribution is consistent with bond length data discussed in section 3.1, and with charge distribution in other mixed (Mn,Co) spinel oxides.[32] The low-temperature behaviour (Fig. 11) indicates a possible antiferromagnetic ordering below *ca.* 12 K. The Curie constant of the lithiated cobalt spinel lies between theoretical values for reduction of manganese (Mn^{4+} to Mn^{3+}) and reduction of cobalt (Co^{3+} to Co^{2+}).

$Li_2Mn_3NiO_8$ shows a large increase in magnetic susceptibility at low temperature, starting at *ca.* 120 K on cooling (see Fig. 12). This feature could be due to the formation of 16d-cation clusters resulting from the strong magnetic frustration in the structure, which prevents spin ordering. This situation is not significatively altered by lithiation: lithium insertion does not modify the 16d sublattice, and the slight bond distances and angles changes do not remove the strong 16d frustration. Note that both Mg^{2+} and low-spin Co^{III} are diamagnetic, so the nickel case is the first one encountered here where all 16d cations contribute to magnetic interactions. The lithiated compound '$Li_4Mn_3NiO_8$' gives the least satisfying agreement between experimental (4.68) and expected (4.396) Curie constant values. This may indicate that lithiation did not proceed to completion (*i.e.* $Li_{<4}$ in the above formula).

Finally, $Li_2Mn_3CuO_8$ (Fig. 13) exhibits a behaviour comparable to the cobalt system, with possible ordering below 12 K. The lithiated compound was not studied in detail, since X-ray diffraction showed that it is strongly disordered.

4 Discussion

The $Li_2Mn_3MO_8$ series is interesting because it allows considerable modification of the manganese valence v(Mn) in $LiMn_2O_4$, while introducing neither vacancies nor distortions.

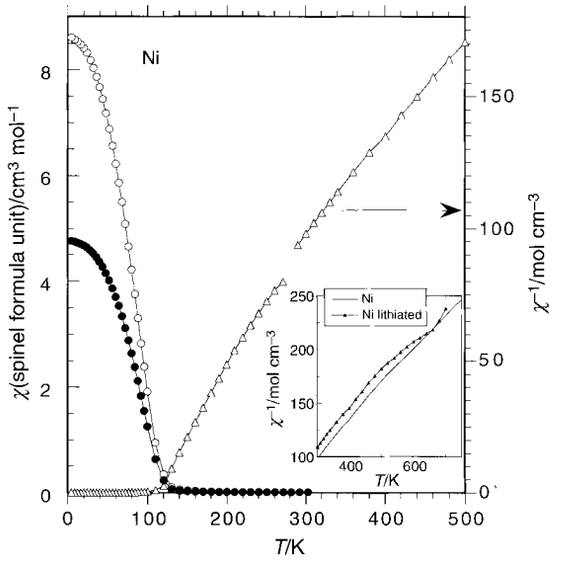

Fig. 12 Temperature dependence of the molar magnetic susceptibility of $Li_{2(1+x)}Mn_3NiO_8$. Data below and above 300 K were measured with fields $H=0.1$ and 4 T, respectively. Open symbols: $x=0$, closed symbols: $x=1$. Inset: susceptibility data up to 750 K.

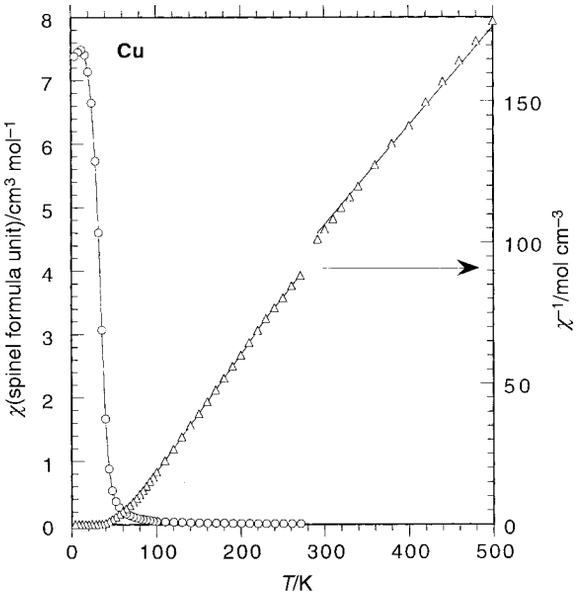

Fig. 13 Temperature dependence of the molar magnetic susceptibility of $Li_2Mn_3CuO_8$. Data below and above 300 K were measured with fields $H=0.1$ and 4 T, respectively.

Table 4 Magnetic susceptibility parameters of $Li_{2(1+x)}Mn_3MO_8$ compounds

M	x	Curie–Weiss law temperature range/K	θ/K	C^a	μ/μ_B	Charge distribution	$C_{expected}$
Mn	0	300–800	−265	4.65	6.10	$Mn^{4+/3+}$	4.875
Mg	0	150–300	+28	2.82	4.75	Mn^{4+}/Mg^{2+}	2.812
Co	0	250–300	−100	3.36	5.18	Mn^{4+}/Co^{2+}	3.750
						$Mn^{4+/3+}/Co^{3+}$ (high spin)	4.875
						$Mn^{4+/3+}/Co^{3+}$ (low spin)	3.375
Co	1	300–500	−271	4.34	5.89	Mn^{3+}/Co^{3+} (low spin)	4.500
						$Mn^{4+/3+}/Co^{2+}$ (low spin)	4.125
Ni	0	500–800	−72	3.34	5.17	Mn^{4+}/Ni^{2+}	3.312
Ni	1	300–500	−52	3.91	4.68	$Mn^{4+/3+}/Ni^{2+}$	4.396
Cu	0	500–800	−24	2.935	4.846	Mn^{4+}/Cu^{2+}	3.00
Cu	1	Non linear					

[a]Per spinel formula (AB_2O_4).

As found previously[6] for $Li_2Mn_4O_9$ and $Li_4Mn_5O_{12}$, both with a high initial manganese valence, electrochemical studies and subsequent X-ray analyses showed that the tetragonal distortion in the $Li_{2+x}Mn_3MO_8$ is negligible for lithiation levels lower than 0.75 Li per AB_2O_4 formula unit, corresponding to $v(Mn) = +3.5$. Interestingly, the cobalt compound follows this general trend, although it was shown to contain 25% Mn^{3+} (charge distribution $[Mn^{4+}{}_2Mn^{3+}Co^{3+}]$).

In spite of this important difference between Li–Mn–O and $Li_2Mn_3MO_8$ spinels, a very similar capacity fade was observed on cycling on the latter, at least for samples prepared by solid state reaction. These results thus question the usually accepted picture attributing performance fading in $LiMn_2O_4$-based electrochemical cells to the occurrence of tetragonal distortion. In fact, the key parameter in electrochemical capacity fading could be rather the oxide morphology (grain size and/or specific surface area), as shown by the remarquable improvement recently reported on sol–gel $Li_2Mn_3NiO_8$ (ref. 11). The evidence of bad kinetics of Li insertion/extraction in solid-state $Li_2Mn_3MO_8$ observed in the present study, even on slow cycling rates ($\approx C/40$), is consistent with that hypothesis. In addition, tetragonal derivatives of $Li_2Mn_3MO_8$ spinels were obtained by chemical lithiation. The extent of lithiation was confirmed by the evolution of Curie constants, while the nature of the magnetic interactions showed little change, as expected from the conservation of the $[Mn_3M]$ sublattice geometry. The magnitude of the tetragonal distortion (see Fig. 14) shows that $Li_2Mn_3MO_8$ spinels with M = Mg, Co or Ni follow the general trend known in the $Li_{1+\alpha+x}Mn_{2-\alpha}O_4$ series.[33] $Li_2Mn_3CuO_8$ is quite atypical in this respect, showing a considerably enhanced tetragonal distortion. This feature can be ascribed to the fact that Cu^{2+} is itself a Jahn–Teller ion (electron configuration $t_{2g}{}^6e_g{}^3$). Consequently, the presence of Cu^{2+} on the 16d sites enhances the Jahn–Teller distortion. Again, we note the absence of any correlation between the increase or decrease in Jahn–Teller distortion for the fully lithiated products and the electrochemically capacity on cycling.

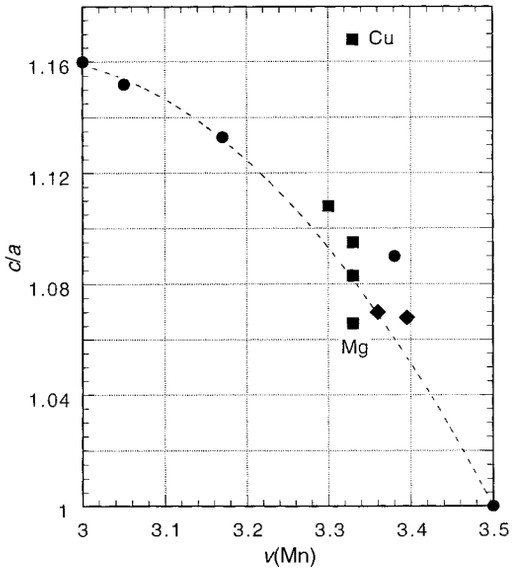

Fig. 14 Evolution of the tetragonal distortion *c/a* in various Li–Mn spinel oxides. Data for chemically lithiated and quenched samples are taken from refs. 22 and 29, respectively.

5 Conclusions

We describe here the preparation, structural and magnetic characterization, and lithium intercalation behaviour of various derivatives of $LiMn_2O_4$. Cationic substitutions on the manganese (16d) site allow to increase the manganese valence, and structural and magnetic measurements confirmed that the stoichiometry expected was reached within experimental error. Rather surprisingly, no improvement in electrochemical cycling performances at 3 V were noted, in spite of the absence of noticeable tetragonal distortion after a few cycles in lithium batteries. Chemical lithiation also showed that the terminal $Li_2(Mn,M)_2O_4$ phases are tetragonal, but with a considerably reduced distortion with respect to $LiMn_2O_4$ for samples with M = Mg, Co or Ni. This study thus questions the possible correlation between electrochemical capacity fade and tetragonal distortion in this system.

Finally, we showed that the magnetism in the $Li_2Mn_3MO_8$ family is dominated by the frustration resulting from the 16d sublattice configuration, which consists in a three-dimensional array of corner-sharing tetrahedra. In the case of M = Ni, clusterization probably occurs below 120 K. Further magnetic studies are in progress on these materials.

Acknowledgements

The authors wish to thank G. Chouteau and E. Chappell (LCMI, Grenoble) for their assistance and helpful discussions on magnetic measurements.

References

1 M. M. Thackeray, *Prog. Batt. Batt. Mater.*, 1992, **11**, 150.
2 D. Guyomard and J. M. Tarascon, *Solid State Ionics*, 1994, **69**, 222.
3 T. Ohzuku, J. Kato, K. Sawai and T. Hirai, *J. Electrochem. Soc.*, 1991, **138**, 2556.
4 M. M. Thackeray, Y. Shao-Horn, A. J. Kahaian, K. D. Kepler, E. Skinner, J. T. Vaughey and S. A. Hackney, *Electrochem. Solid State Lett.*, 1998, **1**, 7.
5 J. Rodriguez-Carvajal, G. Rousse, C. Masquelier and M. Hervieu, *Phys. Rev. Lett.*, 1998, **81**, 4660.
6 M. M. Thackeray, A. de Kock, M. H. Rossouw, D. Liles, R. Bittihn and D. Hoge, *J. Electrochem. Soc.*, 1992, **139**, 363.
7 F. Le Cras, D. Bloch and P. Strobel, *J. Power Sources*, 1996, **63**, 71.

8 F. Le Cras, D. Bloch, M. Anne and P. Strobel, *Solid State Ionics*, 1996, **89**, 203.
9 L. Sánchez and J. L. Tirado, *J. Electrochem. Soc.*, 1997, **144**, 1939.
10 J. Morales, L. Sánchez and J. L. Tirado, *J. Solid State Electrochem.*, 1998, **2**, 420.
11 K. Amine, H. Tukamoto, H. Yasuda and Y. Fujita, *J. Electrochem. Soc.*, 1996, **143**, 1613.
12 F. Le Cras, P. Strobel, M. Anne, D. Bloch, J. B. Soupart and J. C. Rousche, *Eur. J. Solid State Inorg. Chem.*, 1996, **33**, 67.
13 Y. Ein-Eli, W. F. Howard, S. H. Lu, S. Mukerjee, J. McBreen, J. T. Vaughey and M. M. Thackeray, *J. Electrochem. Soc.*, 1998, **145**, 1238.
14 J. Rodriguez-Carvajal, *Satellite Meeting of the 15th Congress of the IUCr*, Toulouse, France, 1990, p. 127.
15 A. H. Thompson, *J. Electrochim. Soc.*, 1979, **126**, 608.
16 J. Barker, *Electrochim. Acta*, 1995, **40**, 1603.
17 C. Bourbon, F. Rouppert, D. Bloch and F. Le Cras, *Fr. Pat. Appl.*, No. 98-0426, 1998.
18 Y. Ein-Eli, J. T. Vaughey, M. M. Thackeray, S. Mukerjee, X. Q. Yang and J. McBreen, *J. Electrochem. Soc.*, 1999, **146**, 908.
19 G. Blasse, *Philips Res. Rep.*, 1964, 1.
20 R. D. Shannon and C. T. Prewitt, *Acta Crystallogr., Sect. A*, 1976, **32**, 751.
21 P. Strobel, F. Le Cras, L. Seguin, M. Anne and J. M. Tarascon, *J. Solid State Chem.*, 1998, **135**, 132.
22 JCPDS card 49-558, 1998.
23 Y. Chabre, in *Chemical Physics of Intercalation II*, ed. P. Bernier, Plenum, New York, 1993, p. 181.
24 T. Ohzuku, A. Ueda and N. Yamamoto, *J. Electrochem. Soc.*, 1995, **142**, 1431.
25 S. Scharner, W. Weppner and P. Schmid-Beurmann, *J. Electrochem. Soc.*, 1999, **146**, 857.
26 C. B. Azzoni, M. C. Mozzati, A. Paleari, V. Massarotti, M. Bini and D. Capsoni, *Z. Naturforsch., Teil A*, 1998, **53**, 771.
27 F. Le Cras, C. Bourbon, D. Bloch, H. Rouault and P. Strobel, *International Battery Association Meeting*, Annecy, France, Oct. 1998, to be published.
28 C. Masquelier, M. Tabuchi, K. Ado, R. Kanno, Y. Kobayashi, Y. Maki, O. Nakamura and J. B. Goodenough, *J. Solid State Chem.*, 1996, **123**, 255.
29 P. Endres, B. Fuchs, S. Kemmler-Sack, G. Faust-Becker and H. W. Praas, *Solid State Ionics*, 1996, **89**, 221.
30 Y. Shimakawa, T. Numata and J. Tabuchi, *J. Solid State Chem.*, 1997, **131**, 138.
31 J. E. Greedan, N. P. Raju, A. S. Wills, C. Morin, S. M. Shaw and J. N. Reimers, *Chem. Mater.*, 1998, **10**, 3058.
32 O. Muller and R. Roy, *The Major Ternary Structural Families*, Springer, Berlin, 1974, p. 252.
33 A. Yamada, K. Miura, K. Hinokuma and M. Tanaka, *J. Electrochem. Soc.*, 1995, **142**, 2149.

Paper a905962h